



Accepted Article

Title: Enhanced Photocatalytic Activity of Molybdate Intercalated Fe-based Layered Double Hydroxide

Authors: Lagnamayee Mohapatra; Dhananjaya Patra; Kulamani Parida; Syed Javaid Zaidi

This manuscript has been accepted after peer review and the authors have elected to post their Accepted Article online prior to editing, proofing, and formal publication of the final Version of Record (VoR). This work is currently citable by using the Digital Object Identifier (DOI) given below. The VoR will be published online in Early View as soon as possible and may be different to this Accepted Article as a result of editing. Readers should obtain the VoR from the journal website shown below when it is published to ensure accuracy of information. The authors are responsible for the content of this Accepted Article.

To be cited as: Eur. J. Inorg. Chem. 10.1002/ejic.201601191

Link to VoR: <https://doi.org/10.1002/ejic.201601191>

Enhanced Photocatalytic Activity of Molybdate Intercalated Fe-based Layered Double Hydroxide

Lagnamayee Mohapatra,^{*a} Dhananjaya Patra,^b Kulamani Parida,^{*c} Syed Javaid Zaidi,^{*a}

^a Center for Advanced Materials (CAM), Qatar University (QU), Doha, Qatar

E-mail: mlagnamayee@gmail.com

Email: szaidi@qu.edu.qa

^b Department of Chemistry, Texas A&M University at Qatar

E-mail: dhananjaya.patra@qata.tamu.edu

^c Centre for Nano Science and Nano-Technology, ITER, Siksha 'O' Anusandhan University, India

E-mail: kulamaniparida@soauniversity.ac.in

Keywords: Photocatalysis, Methyl orange, Degradation, wastewater treatment, Charge separation, Oxo-bridged linkage

Abstract

Herein, we design and successful fabrication of novel Fe-based Mg/Fe Layered double hydroxides (LDHs) with different molar ratios (2:1, 3:1, and 4:1) by co-precipitation method. Among all, the prepared Mg/Fe (4:1) LDH sample with high crystallinity and phase purity was further modified by intercalating molybdate anion. The prepared catalysts were subsequently examined their structural, morphological, optical, electrochemical and photocatalytic properties. In comparison with Mg/Fe (4:1) LDH, the photocatalytic activity for degradation of methyl orange (MO) dye was enhanced surprisingly by intercalating molybdate into the interlayer of Mg/Fe (4:1) LDHs following apparent first order kinetics. The radical trapping experiments demonstrate that h^+ , OH^\bullet and $O_2^{\bullet-}$ radicals are the dominant reactive species for pollutant degradation. The highest photocatalytic activity of molybdate intercalated LDH is attributed mainly to the combined effect of layered structure with Oxo-bridged Mg (II)-O-Fe (III) linkage and intercalated molybdate anion which act as the visible light absorption center towards higher wavelength, and can promote charge carrier trapping, as well as hinder the photogenerated

electron–hole recombination. The time-resolved photoluminescence spectra (TRPL) serves to prolong the charge separation under visible light.

Introduction

Degradation of residual organic dyes from different sources (pharmaceutical industries, textile industries, paper industries, dye and dye intermediates industries, etc.) are becoming one of the most notorious issues in the 21st century for both human beings and ecosystems. Among all chemically synthesized dye-stuffs, azo dyes containing azo groups (R-N=N-R') are unable to noticeably degrade during the biological treatment or any chemical and physical processes. In recent years one of the conventional method is “photocatalysis” based on the advanced oxidation process that can oxidizes the organic pollutants from waste water. Moreover, photocatalysis is one of the green technologies and has been recognized as an effective way to utilize solar energy for destruction of aromatic rings of organic dyes.¹⁻³ Currently, various semiconductor photocatalysts such as SnO₂, CdS, WO₃, In₂O₃, TiO₂, ZnO, ZrO₂, and different layered materials as well as composites have been investigated for photocatalytic demineralization of different pollutants.⁴⁻¹⁶

Layered double hydroxides (LDHs) are found to exhibit good alternatives which have been studied extensively for a wide range of photocatalytic applications possess a layered structure of general formula $[M(II)_{1-x} M(III)_x(OH)_2]^{x+} [A_{x/n} H_2O]^{x-}$, where M(II) and M(III) are metal cations and ‘A’ is an intercalate anion. When divalent cations is substituted by the trivalent cations, the positive charge is generated in the brucite layer and is balanced by the presence of anions in the interlayer space.¹⁷ The brucite layer of LDHs are constituted by sheets of edge shared MO₆ octahedrons and act as a doped semiconductor. Recently, both modified and unmodified LDHs have been reported in the field of selective photocatalysis.¹⁸⁻²⁵

Most polyoxo metalates also showed excellent photocatalytic activity due to their unique electronic structures, crystal structure, energy band structure and charge carriers transfer efficiency.²⁶⁻²⁷ Likewise, incorporation of polyoxometalates in the interlayer region of a layered compound is an encouraging photocatalyst for enhancing the photocatalytic activity.²⁸ The interlayer space of a lamellar semiconductor played a vital role for high catalytic activity.²⁹⁻³⁰ Therefore, introducing polyoxometallates into the interlayer space towards photoactivity is challenging.

In this study, we report fabrication different molar ratios (4:1, 3:1, 2:1) of Mg/Fe LDH and modified it by intercalating molybdate for photo activities. As explained earlier, layered materials use their interlayer space with intercalated anions, edge shared octahedron and Oxo-bridging linkage could retard the electron hole recombination. In an attempt to enhances the light harvesting capacity, and reduce the electron hole recombination with an encouraging results in terms of degradation rate and degradation time, we synthesize molybdate intercalated LDHs. The enhancement of photocatalytic activity of as prepared LDHs has been also explained.

Results and discussion

Structural properties

The XRD patterns of Mg/Fe-2, Mg/Fe-3 Mg/Fe-4 and Mg/Fe-4/Mo LDH catalysts illustrate in Figure 1. This figure reveals the typical reflections of layered double hydroxides with the peaks for d(003) and d(006) at low 2θ angle and the planes for d(101), d(015), d(018), d(110) and d(113) planes at high 2θ angle in case of Mg/Fe-4.^{31,32} In this case, all the reflection peaks ($00l$) could be indexed brucite like structure with the hexagonal unit cells. The basal spacing (sum of one brucite-like layer and interlayer of LDH) corresponding to d (003) was 7.7 \AA ($2\theta \approx 11.4^\circ$). The plane d(003) reflection responds hydrotalcite-type materials and its intensity is associated to the crystallinity degree of the material. In the case of Mg/Fe-3 and Mg/Fe-2, some additional peaks were observed; however, a single crystalline peak was found in Mg/Fe-4 LDH case. The presence of a large amount of Fe^{3+} in the in the salt solution resulted lower crystallinity and less phase purity due to the difference of the ionic radii of the Mg^{2+} and Fe^{3+} . Also the solubility product of " $\text{Mg}(\text{OH})_2$ " is 1.8×10^{-11} far below than that of $\text{Fe}(\text{OH})_3 = 6 \times 10^{-38}$. So, by taking large amount of Fe^{3+} in the salt solution, the product of LDH does not yield single-phase. The degree of crystallinity of Mg/Fe-4 is higher than others. The degree of crystallinity and phase purity are also the significant factors for the photocatalytic activity.³³ For Mg/Fe-4/Mo LDH, the basal spacing value is expanded to 9.7 \AA after intercalation of molybdate (scheme 1). The absence of any peak at 7.7 \AA , which would be the absence of carbonate or nitrate in the interlayer of Mg/Fe-4/Mo. The average crystallite sizes of the materials were calculated using Debye–Scherrer equation,

$$D = 0.9\lambda / (\beta \cos \theta) \quad (1)$$

where D is the average crystallite size, λ is the wavelength of incident X-ray = 1.5418 Å, β is the corrected full width at half-maximum of $d(003)$ reflections, and θ is the diffraction angle for the (hkl) plane.³⁴ The thickness of crystallite sizes towards $d(003)$ plane for Mg/Fe-4 and Mg/Fe-4/Mo are 25.4 and 16.0 nm respectively.

Transmission electron microscopy (TEM) further confirms the architecture of the as-prepared sample Mg/Fe-4 and Mg/Fe-4/Mo (shown as figure 2 a, b). For Mg/Fe-4, the TEM figure revealed that the material consists of typical plate like particle with hexagonal shape with a clean surface; however, Mg/Fe-4/Mo exhibits irregular morphology with uniform dispersion.²⁰ The selected area diffraction (SAED) pattern of materials shows clear diffraction rings verified crystalline nature of Mg/Fe-4, the particle shape is regular hexagonal and the diffraction pattern was very strong, indicating a highly crystalline phase which confirmed from our PXRD section. No any significant change in the morphology of Mg/Fe-4/Mo, even after intercalation of MoO_4^- in the interlayer of LDH. The corresponding SAED pattern is shown in Figure 2(c, d) and this results are in good agreement with the XRD analysis. Figure 2 (e, f) reveals the field-emission scanning electron microscopy (FESEM) images of the Mg/Fe-4 and Mg/Fe-4/Mo LDHs. The image of Mg/Fe-4 shows that the nature of LDH particles, which approximately looks plate-like morphology and stacked on top of each other also some of them are in irregular aggregates. The morphology is not altered after intercalation of molybdate.

Further evidence for the structural confirmation of the synthesized materials were provided by FTIR spectroscopy in the frequency range 4000–500 cm^{-1} (Figure 3). The broad and strong absorption peak between 3600 and 3300 cm^{-1} was due to the stretching vibration of structural –OH groups from LDH layers as well as from the interlayer H_2O molecules. The HOH bending band (ν_2) of water was showed at 1641 cm^{-1} which is also close to that of bulk water. Intercalated carbonate anions gave a strong absorption peak at around 1384 cm^{-1} associated with the carbonate ions which indicates D_{3h} symmetry and only one mode of vibration, which is infrared active. The bands observed below 1000 cm^{-1} such as the M-O-H vibration at 667 cm^{-1} and the O-M-O vibration around 550 cm^{-1} are identified as the lattice vibration modes.³⁵ Furthermore, the stretching vibrations at 665 cm^{-1} is interpreted to Mo–O–Mo. The band at 856 cm^{-1} is related to MoO_4^{2-} and the band at 914 cm^{-1} for Mo =O stretching.³⁶⁻³⁷

The nitrogen sorption isotherm curve confirmed the pore size distribution and surface area of the materials. As can be observed in Figure 1, both the materials exhibit the type IV

isotherm with a distinct H3 type of hysteresis loop based on the standard definition of International Union of Pure and Applied Chemistry (IUPAC). Such a combination of type IV isotherm and type H3 hysteresis loop indicates a characteristic of the mesoporous structure of the material.³⁸ According to Brunauer–Emmett–Teller (BET) analysis, the BET surface area of Mg/Fe-4 and Mg/Fe-4/Mo LDHs was found to be 62 and 84 m²/g, respectively. The increased surface area of Mg/Fe-4/Mo LDH is due to the higher degree of expansion by intercalating MoO₄⁻ in the interlayer of Mg/Fe LDH. The plots of the pore size distribution for analyzing pore size and pore volume of the materials, are investigated by desorption branch of the Barrett-Joyner-Halenda (BJH) method as shown in figure 4 (Inset). The pore size ranging from 3.0 to 50 nm indicates the result of the accumulation of the nanocrystals with mesoporosity. The mesoporosity of the materials allowed rapid diffusion and supplies the efficient transport pathways for the photogenerated charge carriers, which is favorable to the photocatalytic activity.³⁹ The large surface area and porous structure make Mg/Fe-4/Mo LDHs an excellent material toward photocatalysis.

Optical properties

The optical property of catalysts were examined using the UV-Vis DRS. It was carried out to investigate the state of transition metals incorporated into the layered framework and also changes the absorption properties by intercalating the anions in the interlayer region of the LDHs. As presented in figure 5, the broad absorption band in case of Mg/Fe LDH is due to the metal ligand charge transfer band of O_{2p} → Fe³⁺ and the metal-metal-charge-transfer spectra (MMCT) of Mg²⁺-O-Fe³⁺. The MMCT for an oxo-bridged bimetallic system was defined to be an excitation transition of an electron from one metal to the other with different oxidation states, which is known to absorb visible light and even near-IR light. Previously, some groups designated the oxo-bridged systems like Ti^{IV}-O-Cu^I, and Ti^{IV}-O-Ce^{III}, respectively for photocatalysis.^{40,41} Furthermore, parida and coauthors reported the visible-light induced MMCT of different oxo-bridged system towards photocatalysis.^{24,30,42} All results demonstrated that, the hetero-bimetallic oxo-bridged systems induced MMCT and acts as a photo induced redox center.⁴³ In the case of Mg/Fe-4/Mo LDH, the absorption edge shifted towards near IR region is due to the highest occupied molecular orbital to lowest unoccupied molecular orbital (HOMO-

LUMO) oxygen-metal charge transfer spectra (OMCT) of Interlayer molybdate where the HOMO is mainly derived from the O 2p orbitals and the LUMO is from the Mo 4d orbitals.

For a crystalline semiconductor, the optical band gap is calculated by Touc plot:

$$\alpha h\nu = A(h\nu - E_g)^{n/2} \quad (2)$$

Where α, ν , A and E_g are the absorption co-efficient, light frequency proportionality constant and band gap energy, respectively. The values of n and E_g were determined using the published methods.^{42,44} Here, n describes the type of transition in a semiconductor. If n = 1/2 responds for direct transition and n =2 for indirect transition. In our case, the value of n was determined to be 1/2 from their absorption spectra. So, optical transitions for both LDH materials are directly allowed. The band gap energy (E_g) can be estimated from the intercept of the tangents to the plots of $(\alpha h\nu)^2$ against $h\nu$ photon energy as shown in Figure 5(insert figures). The band gap of Mg/Fe-4/Mo (2.06 eV) is indicates a narrow band gap compared to that of Mg/Fe-4 LDH (2.3 eV).

Photoluminescence study

The efficient charge separation and transfer of photo generated exactions are essential for the enhanced photocatalytic activity for a photocatalyst. Photoluminescence (PL) spectroscopy provides the overview of the migration and separation efficiency of charge-carrier trapping, the existence of surface defects and oxygen vacancies of the material. At certain excitation wavelength, the electrons on the valence band (VB) excited to the conductance band (CB) and again back to valence giving rise to PL signal. High PL intensity is considered to reflect a high recombination rate of photogenerated electron hole pairs.⁴⁵ Figure 6 displays the PL spectra of Mg/Fe-4 and Mg/Fe-4/Mo LDH samples in the range of 340–500 nm with the excitation wavelength of 320 nm. All LDH materials showed two strong PL emission peaks at around at 415 nm and 450 nm due to the trapping of charge carriers on its surface and the defect sites of LDHs respectively.^{42,46,47} The pure LDH has a high-intensity emission peak and after intercalating molybdate, the PL signal becomes significantly quenched. A more active separation of electron-hole pairs was observed after incorporation of Molybdate in LDH. This result showed, an efficient charge separation in Mg/Fe-4/Mo LDH, suppressing the recombination of charge carriers and significantly enhanced photocatalytic activities.

Time-resolved photoluminescence study

The recombination of photogenerated excitons (e^- and h^+) can be qualitatively investigated. To determine the lifetime of charge carriers, we have studied the time resolved photoluminescence decay (TRPL) spectra (Figure 7).⁴² The curves have been fitted with bi-exponential decay response functions defined by the following equation^{48, 49}:

$$I(t) = A_1 e^{-\frac{t}{\tau_1}} + A_2 e^{-\frac{t}{\tau_2}} \quad (3)$$

which contains two lifetimes (τ_1 and τ_2), and the corresponding amplitudes (A_1 and A_2). The intensity average lifetime of both the materials were calculated to make an overall comparison of the emission decay behavior. The calculated average lifetimes of Mg/Fe-4 is 310 ps and Mg/Fe-4/Mo is 980 ps (Table 1). This result demonstrates that, HOMO-LUMO transitions of interlayer molybdate prohibit the recombination of electron and holes. Both the results of PL showed that with Mg/Fe-4/Mo LDH, the PL intensity as well as the time period for charge separation are improved, which are very promising result for the photocatalytic reactions.

Photo electrochemical properties

To better understand the mechanism, we further investigated the photoelectrochemical properties of the material by photocurrent measurement. The result of photocurrent measurements for both the materials confirmed that both are p-type semiconductor and serving as photocathodes [figure 8(a)]. The photocurrent onset potentials (valence band edge) of both Mg/Fe-4 LDH and Mg/Fe-4/Mo LDH were observed at +2.04V and +2.14 V vs. Ag/AgCl at pH 6.5. In our case Mg/Fe-4/Mo LDH (+2.14V) showed a higher oxidation ability (more positive valence band potential) than Mg/Fe-4 LDH (+2.08V) which are more positive than OH^\bullet/OH^\ominus (1.19V) and suggesting that both could ability to produce OH radical.^{43,50} Furthermore, we have done the EIS analysis to recognize the charge transfer properties. Figure 8(b) shows EIS Nyquist plots of Mg/Fe-4 and Mg/Fe-4/Mo LDH electrodes. It could be seen that, in the presence of visible light irradiation, the diameter of the Nyquist circle of Mg/Fe-4/Mo was significantly lower than that of the pristine Mg/Fe-4 LDH. The smaller diameter of the arc implied lower charge transfer resistance and enhance the separation and transfer efficiency of photogenerated electron and holes, which corresponds superior photocatalytic activity.⁵¹ This result demonstrates that the intercalation of molybdate in Mg/Fe-4 LDH can dramatically enhance the photocatalytic efficiency.

Catalytic activities

The photocatalytic activities of Mg/Fe-4 and Mg/Fe-4/Mo LDH samples were investigated by degrading organic pollutant like methyl orange (MO) under solar light ($\lambda > 400$ nm) irradiation. Figure 9 (a) showed the rate of decolorized of MO over Mg/Fe-4 and Mg/Fe-4/Mo LDH materials. As the highest chemical stability of MO, the photolysis of the dye (without catalyst) under visible irradiation was negligible. Prior to photocatalytic experiment, the adsorption properties of MO over two as prepared catalysts were examined in the dark condition up to 30 minutes. The adsorption/desorption equilibriums of the dye over two samples are totally established within that time period. With respect to the same initial MO concentration, only 15% and 20% MO are adsorbed over Mg/Fe-4 LDH and Mg/Fe-4/Mo LDH, respectively, indicating that Mg/Fe-4/Mo showed high adsorption ability to adsorb MO in aqueous solution due to high basal spacing corresponding high surface area. Then the solution was stirred under visible light irradiation for photocatalytic reaction. The result directed that, Mg/Fe-4/Mo presented the most impressive photocatalytic degradation ability, and completely decomposed MO dye molecules within 60 min. By contrast, at the same reacting time, the removal rate of MO dye over Mg/Fe-4 was only ~60% and about 90% decomposed after 180 minutes. The excellent photocatalytic activity was showed in the case of Mg/Fe-4/Mo LDH under solar-light irradiation.

Correspondingly, different experiments were investigated using the initial MO concentrations varying from 50 mg/L to 100 mg/L with materials doses 1g/L to know the effect of concentration of dye in the degradation process over Mg/Fe-4/Mo LDH. The photo degradation rate of MO was about 90% degradation rate in case of both cases (50 mg/L, 80mg/L initial dye concentration) and 48.39% degradation rate in case of 100mg/L initial dye concentration.⁴⁴ At higher dye initial concentration, the approach of the radiation of photons to the catalyst surface is hindered, thereby, reducing the photocatalytic activity. So we carried out all the reactions in 80ppm dye concentration with 1g/L materials doses. As methyl orange dye regarded as an anionic dye and the point of zero charge (PZC) of both the LDHs are 7.5 and 8.0. When $P^H > PZC$, the surface of the catalyst exhibit a negative charged surface and the below PZC, the MO dye can adsorbed in to the surface of the catalysts easily via coulombic interaction. Hence, the weak acid or neutral is the ideal condition for MO degradation over LDHs. So we proposed that the best range of pH for MO degradation was under weak acid condition. Furthermore, the structure of layered materials with hydroxide sheets is vanished below pH 3.

52,53

In addition, the kinetic curve of MO photocatalytic degradation was also investigated by fitting its kinetic curve according to an approximated pseudo-first-order process. Figure 9 (b) showed the plots of $\ln(C_0/C)$ versus irradiation time and the fitting results of these plots.

$$\ln(C_0/C) = k_{app}t \quad (4)$$

where C is the instantaneous concentration of MO solution at time t (mol/L), C_0 is the initial MO concentration (mol/L), and k_{app} is the apparent pseudo-first-order rate constant (min^{-1}).

The $t_{1/2}$ parameters which indicates the time required to degrade half of the initial concentration of dye can be calculated by using the following equation:

$$t_{1/2} = 0.693/k_{app} \quad (5)$$

The apparent reaction rate constant k_{app} and $t_{1/2}$ for the sample Mg/Fe-4 and Mg/Fe-4/Mo LDH was 0.021 min^{-1} ($t_{1/2} = 32 \text{ min}$), and 0.057 min^{-1} ($t_{1/2} = 11 \text{ min}$) respectively, suggesting a preferable photocatalytic performance of the sample Mg/Fe-4/Mo LDH.

The stability of the materials were evaluated by recycling the photocatalysts for the degradation of MO under visible irradiation for 3 hours. After each run, the fresh MO dye solution was used for each photocatalytic experiment. Also the catalysts were collected, washed and then reused. As shown in Figure 9(c), there was no significant decrease of the efficiency after four successive cycles, the photocatalytic efficiency decreased only slightly after four successive cycles, indicating that the photocatalysts were photo- and chemically stable.

The chemical oxygen demand (COD) was widely used to measure the organic strength of the organic pollutant which indicate the mineralization of methyl orange dye. In our case, COD method was performed by acidic dichromate method. Figure 9(d) shows the disappearance of COD with respect to time. It can be seen that there is a gradual reduction in the COD values and the efficiency of COD was about maximum of 70% and 80% efficiency for Mg/Fe-4 LDH and Mg/Fe-4/Mo LDH respectively.^{32,43}

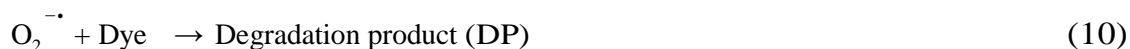
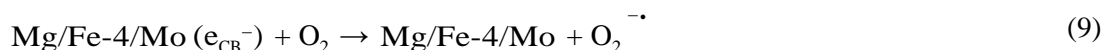
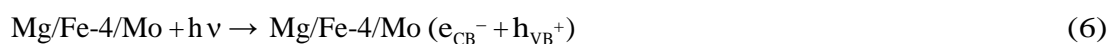
Mechanistic Aspects

Mg/Fe LDH constitute the sheets of edge shared Mg (OH)₆ and Fe(OH)₆ octahedral units. In FeO₆, the top of the VB is mainly composed of O 2p orbital and the bottom of the CB Fe³⁺ (3d orbital). When a semiconductor photocatalyst (Mg/Fe-4 LDH) is exposed by photon of energy equal to or greater than the band-gap energy, the valence band electron of O 2p orbital of FeO₆ was excited to the conduction band of Fe³⁺ (3d orbital) resulting hole and electron in the valence band and conductance band respectively. The photogenerated holes are trapped by surface

absorbed water to form hydroxyl radicals (OH^\bullet), and the photogenerated electrons are absorbed by oxygen to form super oxide radicals ($\text{O}_2^{\bullet-}$).²⁵ The hydroxyl radical and superoxide radicals are active species helps for photodegradation of organic pollutants.

As LDHs has cation doping capacity at the MO_6 octahedrons of brucite layers, consequently it act as a doped semiconductor toward photocatalysis and the higher valent cation act as a dopant. Recently, the photocatalytic performance of the Fe doped semiconductor have been investigated many groups.⁵⁴ Recent study explained the photo functional LDHs with ternary cations were demonstrated as an effective dopant to show excellent results towards photocatalysis. Also, the good crystallinity of LDHs can be the essential factor for photocatalysis which depends upon various metal cations and interlayer anions as well as different metal ratios.⁵⁵

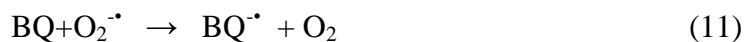
According to the Kabakcioglu density functional theory, the molybdate bearing Td symmetry with highest occupied molecular orbital (HOMO) which is nonbonding fully filled oxygen 2p orbital and lowest unoccupied molecular orbital (LUMO) contributing Mo (4d orbital).⁵⁶ This study also confirmed that, when Mg/Fe-4/Mo photocatalyst absorbed photon energy under visible light irradiation, the excited electron induces oxygen-metal charge transfer spectra (OMCT) which has a high oxidizing power to oxidize dye compounds can be represented as follows and schematically represented in scheme 2:



Investigation of active species:

The significantly enhanced photocatalytic activity of the Mg/Fe-4/Mo LDHs catalysts motivated us to investigate the active species in degradation process. Generally, photo induced holes (h^+), hydroxyl radicals (OH^\bullet) and superoxide radicals ($\text{O}_2^{\bullet-}$) are the main reactive species involved in the photocatalytic degradation of dyes. Hence the trapping experiments were conducted (as shown in figure 10) by taking various scavengers, including disodium salt of

ethylene-diamine-tetra-acetic-acid (Na₂-EDTA) for holes (h⁺), benzoquinone (BQ) for superoxide radicals, and isopropanol (IPA) for hydroxyl radicals (OH[·]) for detecting the active species in the photodegradation of MO dye. When holes (h⁺) reacts with oxalate ion, it produced active carbondioxide anion radical and hence can reduce degradation process. Similarly, benzoquinone and isopropanol (IPA) inhibit the degradation process.



The % of MO degradation was significantly decreased by adding IPA, indicating that OH radicals were foremost active species in this photo degradation reaction. Likewise, the addition of Na₂-EDTA and BQ decreased on the degradation of MO, confirming that the holes and superoxide radicals were also dominant active species. The above results confirmed that the degradation process was mainly owing to direct holes, OH[·] and O₂^{·-} radicals.⁴³

Factors Affecting the Photocatalytic Degradation

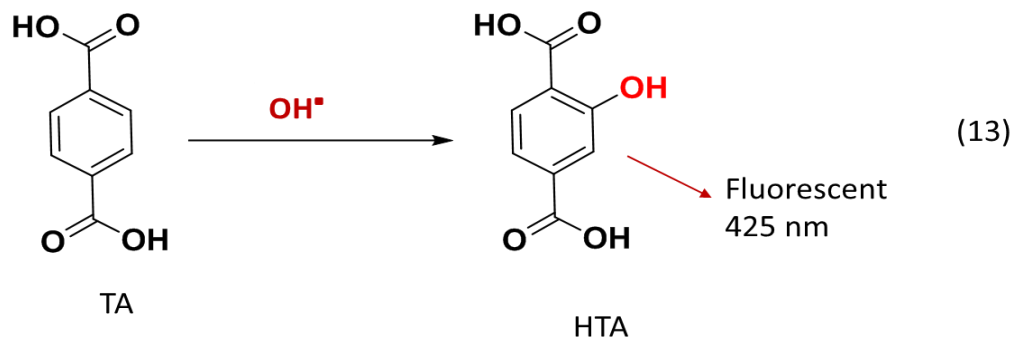
1. Oxo bridged system

A feature of the structure of LDH is the connecting of different metal ions to each other by oxygen atoms having different metal- oxygen- metal sites. The metal- oxygen- metal sites of LDHs reduce charge recombination via a metal-to metal charge transfer (MMCT) mechanism. In the pioneering work by Fri groups, a variety of oxo-bridged systems have been developed for photocatalysis.⁴¹ The visible light photo excitation of MMCT transition was followed by electro transfer from one metal to another metal (acceptor), which result in the formation of transition species. The MMCT of the oxo bridged system are suitable for the photocatalysis. MMCT groups act as visible light active electron pumps with adjustable redox potential that depends upon the selected donor acceptor metals and its oxidation states. Fe-based Oxo-bridging LDH photocatalysts help to prevent the recombination of charge carriers and enhanced the photo activity.⁵⁷

2. Generation of the Hydroxyl Radical

The hydroxyl radical plays an important role for the degradation of the organic dyes. Henceforth, it is crucial to investigate the generation of hydroxyl radicals formed by each photocatalyst. Terphthalic acid (TA) by using PL technique is used as a probe molecule for

detection of OH^\bullet radicals. The PL emission spectrum excited at 315 nm of the solution containing TA and when it reacts with OH^\bullet radicals, produced 2-hydroxyterephthalic acid (TAOH) and gives a fluorescence signal at 425 nm (equation 13).⁴² Figure 11 illustrates the changes of PL spectra of all the as prepared materials after reaction. It can be revealed that, the PL intensity is larger in case of Mg/Fe-4/Mo LDHs than the Mg/Fe-4 LDHs at wavelength range of 350–550 nm. According to recent reports, the signal of PL is only caused by the reaction of TA with $\bullet\text{OH}$ radicals formed on the photocatalyst during visible-light irradiation and the PL intensity is directly associated to the number of hydroxyl radicals produced by the photocatalysts.⁵⁸ Thus, the highest PL intensity of Mg/Fe-4/Mo LDH confirms the generation of a more number of hydroxyl radicals gives fruitful result compared to Mg/Fe-4 LDH photocatalyst.



3. Lowering of Electron–Hole Recombination and prolonged charge carriers

The photocatalytic activity of the photocatalyst and the separation efficiency of the photo-generated charge carriers are closely related. The PL emission spectra mostly result for the recombination of e^- and h^+ charge carriers of the semiconductor. In the case of the Mg/Fe-4/Mo, the PL signal becomes significantly quenched after intercalating molybdate. This is due to the intercalated molybdate ion. The highest quenching indicating the lower degree of recombination of the electron–hole pairs with the highest photocatalytic activity. Moreover, the increase of the photoluminescence lifetime can be inversely related to the radiative recombination of charge carriers.⁵⁹ From TRPL analysis, we concluded that, Mg/Fe-4/Mo LDH has about 3 times longer decay time than Mg/Fe-4 LDH. The longevity of long lived charge carriers are beneficial for the photocatalytic reactions.

4. Generation of High Photocurrent and lower charge transfer resistance

The higher the applied potential, the higher the photocurrent generated by the samples. The Mg/Fe-4/Mo LDH has higher photocurrent density as compared to Mg/Fe-4 LDH implies that, the availability of photoelectrons is responsible for the degradation of dyes. Hence, the interlayer molybdate play an important role for increasing the photocurrent density as well as increasing the effective charge carriers' separation and improve photocatalytic activity. Also the higher oxidation ability of Mg/Fe-4/Mo LDH attributed to the high MO dye degradation.

Conclusions

In this work, we have successfully synthesized the visible light-driven Mg/Fe-4LDH and molybdate intercalated Mg/Fe-4 LDH and their photocatalytic activity towards photocatalytic MO dye (100ppm) degradation investigated. The photocatalytic result indicate that the Mg/Fe-4 LDH sample possess 90(%) degradation after 3hrs whereas Mg/Fe-4/Mo LDH can absolutely degrade within 45 minutes under simulated visible light irradiation. The materials have good stability and have demonstrated easy reusability with easy reusability and good stability. The superior result was attributed due to the synergistic effect of high band gap energy, ability to utilize broad bands in the solar spectrum and high surface area. On the basis of the active species trapping experiments, photoluminescence study and the photo electrochemical measurements, the factors of enhanced photo activity of the Mg/Fe-4/Mo LDH was discussed. The prolonged lifetime of photogenerated charge carriers and faster interfacial charge-transfer rate of Mg/Fe-4/Mo LDH could improve photo activity. These modified photo catalysts can be reused easily several times without substantial loss of the activity, which is alternative green material towards degradation of organic dyes. This work can be a basis for future work for designing other novel intercalating materials with remarkable properties, for applications in photocatalytic degradation of different organic pollutants, photocatalytic water splitting to produce hydrogen, photocatalytic CO₂ conversion to future renewable fuels.

Experimental Section

The Mg/Fe LDH materials used in this study were prepared by co-precipitation process i.e. a mixed Mg(NO₃)₃.6H₂O and Fe(NO₃)₂.6H₂O solution with Mg/Fe desired M (II)/M (III) molar ratios (4:1,3:1,1:1) were titrated drop wise with sodium hydroxide (1.0 M) mixed alkali with vigorous stirring at room temperature (35±2⁰ C) up to pH 9.0. The resulting suspension transferred to the Teflon coated stainless steel autoclave for hydrothermal treatment at 1200C for 10 h, then filtered and washed with deionised water until the pH of the filtrate was around 7.0

and then dried at 60°C for 24 h. LDHs prepared with variation of molar ratios 4:1, 3:1 and 2:1 are named as Mg/Fe-4, Mg/Fe-3 and Mg/Fe-2. The details of the preparation procedure of intercalated MoO₄⁻ anions over Mg/Fe-4 LDHs has been reported elsewhere.³¹

The samples were characterized by powder X-ray diffraction (PXRD) measurements, high resolution transmission electron microscopy (HRTEM), field emission scanning electron microscopy (FESEM), Fourier transform infrared (FTIR) spectra, diffused reflectance UV-vis (DRUV-vis) spectra, photoluminescence (PL) spectra, time resolved photoluminescence (TRPL) spectra. Rigaku Miniflex was used to record the powder X-ray diffraction (PXRD) ranging from 3° to 70° with a scan rate of 5°/min using Cu K α radiation ($\lambda = 1.54\text{\AA}$). Transmission electron microscope images were carried out by TEM FEI, TECNAI G 20, and TWIN at 200 kV and FESEM images were obtained using a HITACHI 3400N microscope. The Fourier transform infrared (FTIR) spectra of the samples were recorded on a Varian FTIR spectrophotometer. BET surface areas of the samples were analyzed by the multipoint N₂ adsorption-desorption method at liquid nitrogen temperature in a constant-volume adsorption apparatus (BELSORP-mini, BEL JAPAN). UV-vis (DRUV-vis) spectra of the catalyst samples were taken with Varian Cary IE UV-vis spectrophotometer. Photoluminescence spectral measurements were performed on a Perkin-Elmer (LS 55) fluorescence spectrophotometer. Time-resolved photoluminescence (PL) spectra were measured at room temperature using a Fluoromax-4 spectrofluorometer (HORIBA Scientific). The photocurrent and electrochemical impedance spectroscopy (EIS) were measured with an electrochemical analyzer (CHI 660B Chenhua Instrument Company).

Photo electro chemical experiments, the Mg/Fe-4 and Mg/Fe-4/Mo LDH film electrodes were prepared by electrophoretic deposition by the previous method by using a potentiostat (ITECH IT6834). The current potential measurements were carried in a three-electrode electrochemical cell with Ag/AgCl electrodes, a platinum wire and the prepared electrode were used as reference, counter, and working electrodes, respectively. The potential of the working electrode was controlled by a potentiostat and the cell was filled with an aqueous solution of Na₂SO₄ (0.1 M) at pH around 6.5. A scanning potentiostat (Gamry 3000) was used to measure photo currents at a scan rate of 10 mV/s. A 100 W ozone-free xenon lamp (Abet Technologies, USA) was used as the light source, with simulate sunlight at 100mW/cm². The Nyquist plots were recorded within 100 MHz to 100 kHz frequency range.

For a typical photocatalytic experiment, 20 mg of catalyst was added to an aqueous solution of methyl orange (usually 20 ml of 80 ppm) in different 100 ml quartz reactors. A 500 W Xe lamp was used as the light source with a 420 nm cut-off filter and the measured light intensity of 120 mW cm². Prior to irradiation, the suspension was magnetically stirred under dark for 30 minute to establish the adsorption and desorption equilibrium, then suspension were exposed to lamp for 180 minutes. After irradiation, the suspension was centrifuged and the dye content was concentration of the dye was monitored using a UV-visible spectrometer (Cary 100 model EL 96043181) at different time intervals and the blank reaction was also carried out by the same procedure without adding any catalyst named as photolysis reaction. The absorbance at 450 nm was used for estimating the concentration of the methyl orange dye. And the degradation of dye is expressed by C/C_0 , where C_0 is the residual concentration and C is the initial concentration of the dye.

Acknowledgements

This work is financially supported by Center for advanced materials, Qatar University.

References

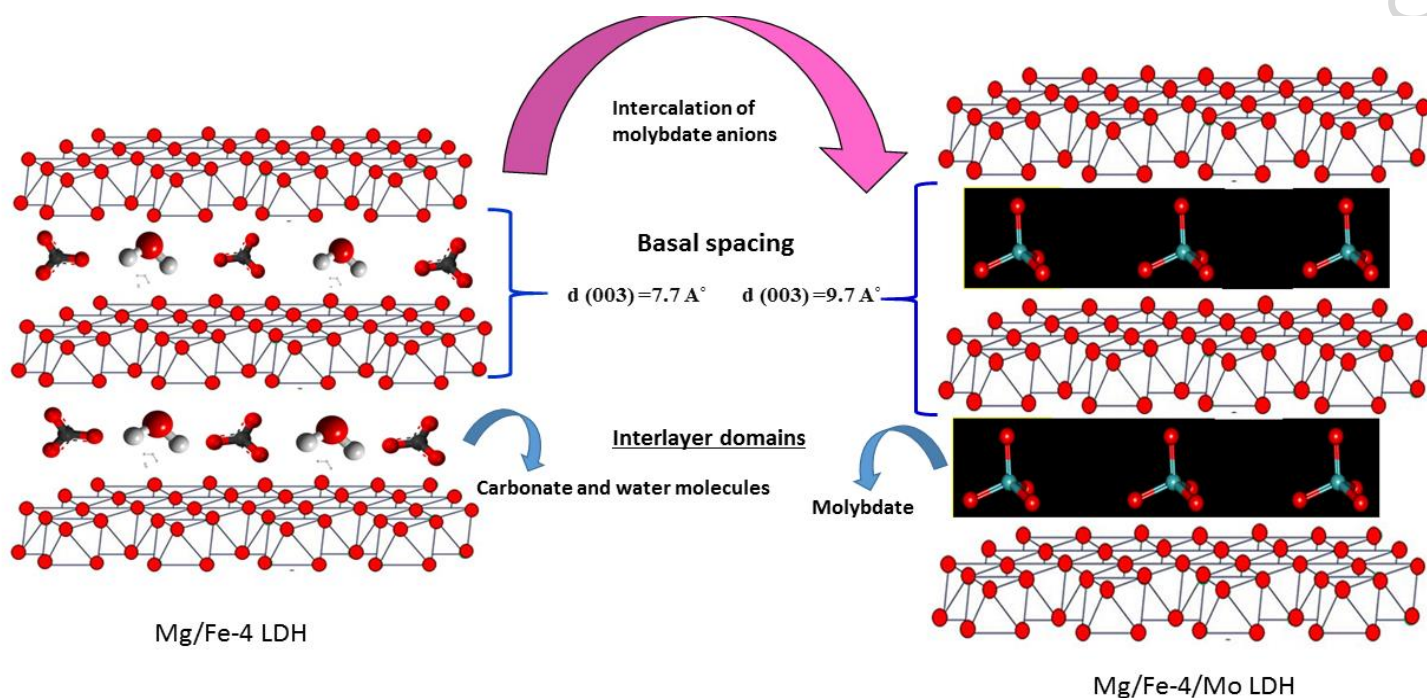
1. M. R. Hoffmann, S. T. Martin, W. Choi, D. W. Bahnemann, *Chem. Rev.*, 1995, **95**, 69–96.
2. H. Kisch, *Angewandte Chemie International Edition*, 2013, **52**, 812–847.
3. H.Tong, S. Ouyang, Y.Bi, N. Umezawa, M. Oshikiri, J.Ye, *Advanced Materials*, 2012,**24**, 229–251.
4. A. Gupta, J.R. Saurav, S. Bhattacharya, *RSC Adv.*, 2015, **5**, 71472–71481.
5. Y.Zheng, L. Lin, B. Wang, X. Wang, *Advanced Materials*, 2015, **54**, 12868–12884.
6. I.Y. Kim, J. M. Lee, T. W. Kim, H. Na Kim, H. Kim, W. Choi, S.-Ju Hwang, *small*, 2012,**8**, 1038–1048.
7. W. J Hye, C. Seung-Yo, H.H. Seong, L. Sang Kyoo, H. Dong Suk, A-W Ahmed, P. Hyunwoong, *J. Phys. Chem. C*, 2014, **118**, 21331–21338.
8. B. Naik, K. M. Parida C.S. Gopinath, *J. Phys. Chem. C*, 2010,**114**, 19473–19482.

9. S. Martha, D. P. Das, N. Biswal, K. M. Parida, *Journal of Materials Chemistry*, 2012, DOI: 10.1039/c2jm30462g.
10. J. Xu, B. Yang, M. Wu, Z. Fu, Y. Lv, Y. Zhao, *J. Phys. Chem. C*, 2010, **114**, 15251–15259.
11. Y. Cao, T. He, Y. Chen, Y. Cao, *J. Phys. Chem. C*, 2010, **114**, 3627–3633.
12. B Naik, K. M. Parida, *Ind. Eng. Chem. Res.*, 2010, **49**, 8339–8346.
13. Q. Wang, Y. Shi, Z. Du, J. He, J. Zhong, L. Zhao, H. She, G. Liu, B. Su, *Eur. J. Inorg. Chem.*, **2015**, 4108–4115.
14. Z. Li, Z. Ren, Y. Qu, S. Du, J. Wu, L. Kong, G. Tian, W. Zhou, H. Fu, *Eur. J. Inorg. Chem.*, **2014**, 2146–2152.
15. K. M. Parida, S. Martha, D. P. Das, N. Biswal, *J. Mater. Chem.*, 2010, **20**, 7144–7149.
16. G. K. Pradhan, S. Martha, K. M. Parida, *ACS Appl. Mater. Interfaces*, 2012, **4**, 707–713.
17. A. Mantilla, F. Tzompantzi, J.L. Fernandez, *Catalysis Today*, 2009, **148**, 119–123.
18. B. Grégoire, C. Ruby and C. Carteret, *Dalton Trans.*, 2013, **42**, 15687–15698.
19. A. Mantilla, G. J. Acatitla, G. M. Mendoza, F. Tzompantzi, R. Gomez, *Ind. Eng. Chem. Res.*, 2011, **50**, 2762–2767.
20. C. Silva, Y. Bouizi, V. Fornes, H. Garcia, *J. Am. Chem. Soc.*, 2009, **131**, 13833–13839.
21. G. Carja, A. Nakajima, S. Dranca, C. Dranca, K. Okada, *J. Phys. Chem. C*, 2010, **114**, 14722–14728.
22. K.M. Parida, M. Satpathy, L. Mohapatra, *J. Mater. Chem.*, 2012, **22**, 7350–7357.
23. Y. Zhao, S. Zhang, B. Li, H. Yan, S. He, L. Tian, W. Shi, J. Ma, M. Wei, D. G. Evans, *Chem. Eur. J.*, 2011, **17**, 13175.
24. J. Fahel, S. Kim, P. Durand, E. Andréa, C. Carteret, *Dalton Trans.*, 2016, DOI: 10.1039/c6dt00441e.
25. K. M. Parida, L. Mohapatra, N. Baliarsingh, *J. Phys. Chem. C*, 2012, **116**, 42417–22424.
26. K. M. Parida and L. Mohapatra, *Dalton Trans.*, 2012, **41**, 1173.
27. R. O. Ruya, J. L. Ferry, *Environ. Sci. Technol.*, 2001, **35**, 3242–3246.
28. A. Dolbecq, P. Mialane, B. Keita, L. Nadjo, *J. Mater. Chem.*, 2012, **22**, 24509–24521.
29. J.L. Gunjekar, T.W. Kim, I.Y. Kim, J.M. Lee, S.-J. Hwang, *Sci Rep.*, 2013, **3**: 2080, 1–8.
30. A. Kudo, A. Tanaka, K. Domen, K. Maruya, K. Aika, T. Onishi, *J. Catal.* 1988, **111**, 67 – 76.

31. L. Mohapatra, K. M. Parida, M. Satpathy, *J. Phys. Chem. C*, 2012, **116**, 13063- 13070.
32. Y. Peng, W. Wang, J. Cao, X. Guo, *RSC Adv.*, 2015, **5**, 41230–41237.
33. Q. Wang, T. Hisatomi, Y. Moriya, K. Maeda, K. Domen, *Catal. Sci. Technol.*, 2013,**3**, 2098- 2103.
34. L. Alexander, H. P. Klug, *Journal of Appl. Physics*, 1950, **21**, 137-142.
35. Y. Chuang, Y. Tzou, M. K. Wang, C. H. Liu and P. N. Chiang, *Ind. Eng. Chem. Res.* 2008, **47**, 3813-3819.
36. V. Christophe, G.-D. Liliane, D. Alain, L. Florian, F. David, D. Claude, *J. Mater. Chem.* 2002, **12**, 1035–1043.
37. A. Davantes, G. Lefevre, *J. Phys. Chem. A* 2013,**117**, 12922–12929.
38. H. Choi, A. C. Sofranko, M. G. Antoniou, M. Pelaez, A. A. dela Cruz, J. A. Shoemaker, D. D. Dionysiou, *Environ. Sci. Technol.* 2007, **41**, 7530–7535.
39. Choi, S. K.; Kim, S.; Lim, S. K.; Park, H. *J. Phys. Chem. C*, 2010, **114**, 16475–16480.
40. Li, Z.; Dai, Y.; Ma, X.; Zhu, Y.; Huang, B. *Phys. Chem. Chem. Phys.*, 2014, **16**, 3267-3277.
41. W. Lin and H. Frei, *J. Phys. Chem. B*, 2005, **109**, 4929- 4935.
42. L. Mohapatra, K. M. Parida, *Phys. Chem. Chem. Phys.* 2014, **16**, 16985- 16996.
43. A. G.Vargas, E. Lima, G. A. Uriostegui-Ortega, M. A. Oliver-Tolentinoc, E. E. Rodríguez, *Applied Surface Science*, 2016,**363**, 372–380.
44. L. Huang, J. Yang, X. Wang, J.-f. Han, H. Hana, Li. Can, *Phys. Chem. Chem. Phys.*, 2013, **15**, 553-560.
45. X. Liua, L. Pana, Q. Zhao, T. Lva, G. Zhua, T. Chena, T. Lua, Z. Suna, C. Sun, *Chemical Engineering Journal*, 2012, **183**, 238–243.
46. Pradhan, G. K.; Padhi, D.K.; Parida, K. M. *ACS Appl. Mater. Interfaces* 2013, **5**, 9101–9110.
47. Yang, T. T.; Chen, W. T.; Hsu, Y. J.; Wei, K. H.; Lin, T. Y.; Lin, T. W. *J. Phys. Chem. C*, 2010, **114**, 11414.
48. M. Soni, S. K. Das, P. K. Sahu, U. P. Kar, A. Rahaman, M. Sarkar, *J. Phys. Chem. C*, 2013, **117**, 14338-14347.
49. J. Shi, J. Chen, Z. Feng, T. Chen, X. Wang, P. Ying, C. Li, *J. Phys. Chem. B*, 2006, **110**, 25612-25618.

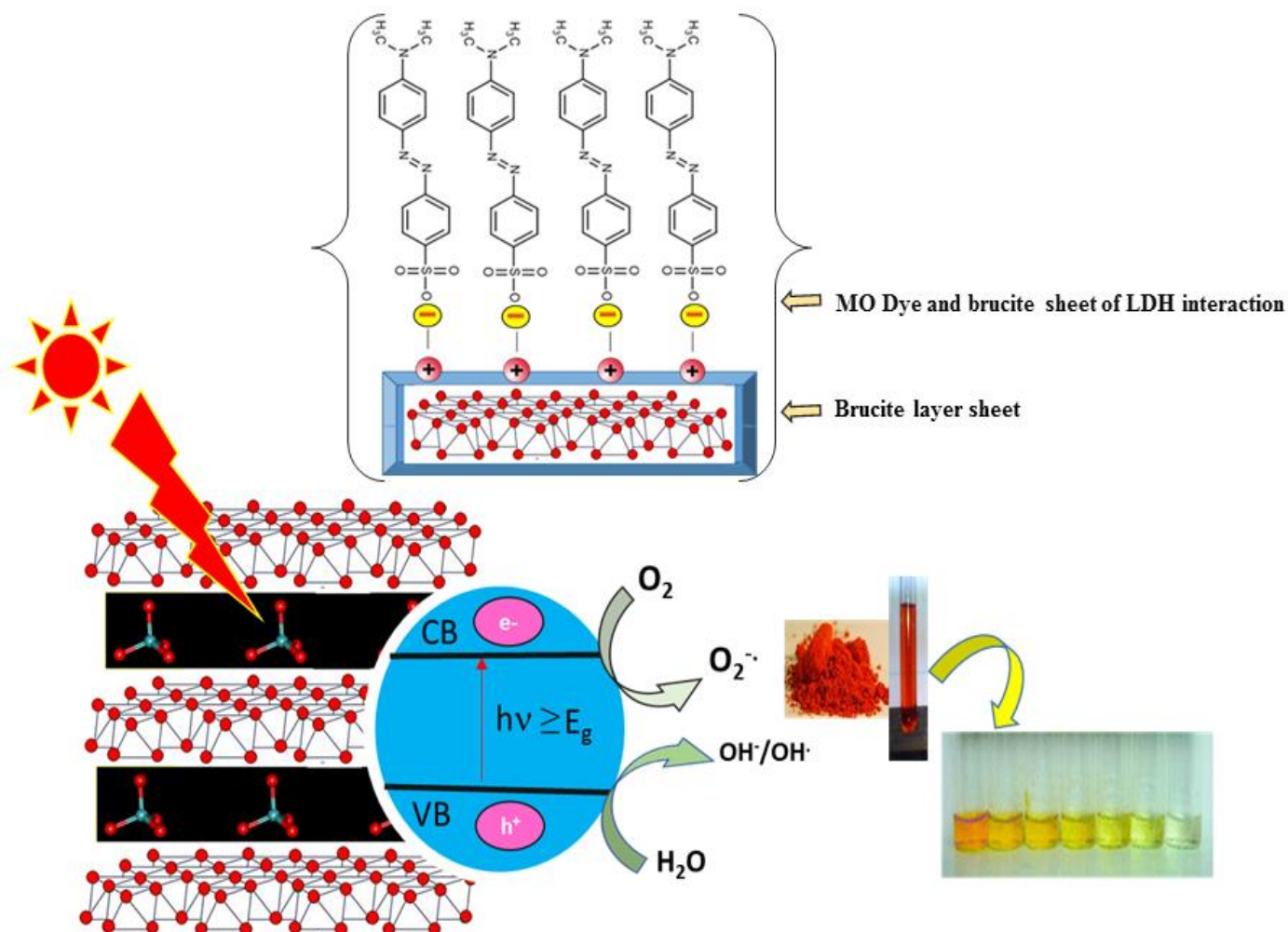
50. S. Zheng, J. Lu, D. Yan, Y. Qin, H. Li, D. G. Evans, X. Duan, *Scientific Reports*, 2015, **5**, 12170.
51. K.M. Parida, L. Mohapatra, *Chemical Engineering Journal*, 2012, **179**, 131–139.
52. L. Mohapatra, K.M. Parida, *J. Mater. Chem. A*, 2016, **4**, 10744-10766.
53. Hao, S.; Hou, J.; Aprea, P.; Lv, T. *Ind. Eng. Chem. Res.*, 2014, **53**, 14617–14622.
54. Liu, M.; Qiu, X.; Miyauchi, M.; Hashimoto, K. *J. Am. Chem. Soc.*, 2013, **135**, 10064–10072.
55. N. Baliarsingh, K. M. Parida, G. C. Pradhan, *Ind. Eng. Chem. Res.* 2014, **53**, 3834–3841.
56. S. Xu, J. Shen, S. Chen, M. Zhang, T. Shen, *J. Photochem. Photobiol. B*, 2002, **67**, 64-70.
57. S. J. Kim, Lee, Y.; Lee, D. K.; Lee, J. W.; Kang, J.K. *J. Mater. Chem. A*, 2014, **2**, 4136-4139.
58. Y. Nosaka, S. Komori, K. Yawata, T. Hirakawa, A. Y. Nosakaa, *Phys. Chem. Chem. Phys.* 2003, **5**, 4731-4735.
59. L. Huang, Y. Jinhui, X. Wang, J. Han, H. Han and C. Li, *Phys. Chem. Chem. Phys.*, 2013, **15**, 553-560.

Schemes



Scheme 1. Schematic representation of nitrate/carbonate exchange with Molybdate ion in layered double hydroxide; Basal spacing calculated from XRD analysis.

Accepted Manuscript



Scheme 2. Schematic representation of detailed the interaction of dye with LDH and the degradation mechanism over Mg/Fe-4/Mo LDH.

Figures

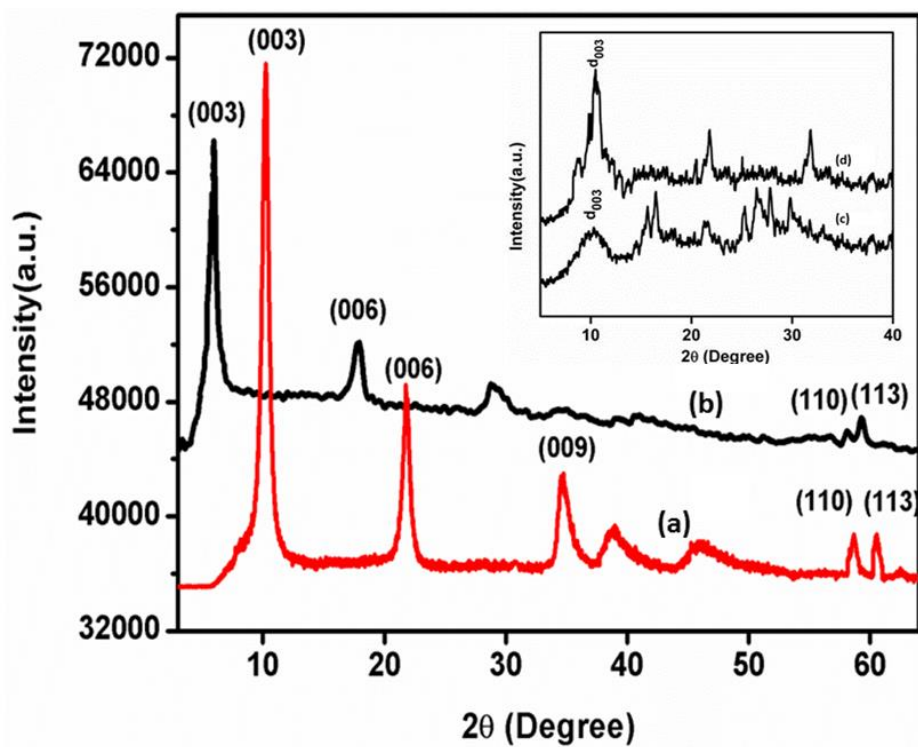


Figure 1. X-ray diffraction patterns of (a) Mg/Fe-4 LDH (b) Mg/Fe-4/Mo LDH(c) Mg/Fe-3 LDH (d) Mg/Fe-2 LDH.

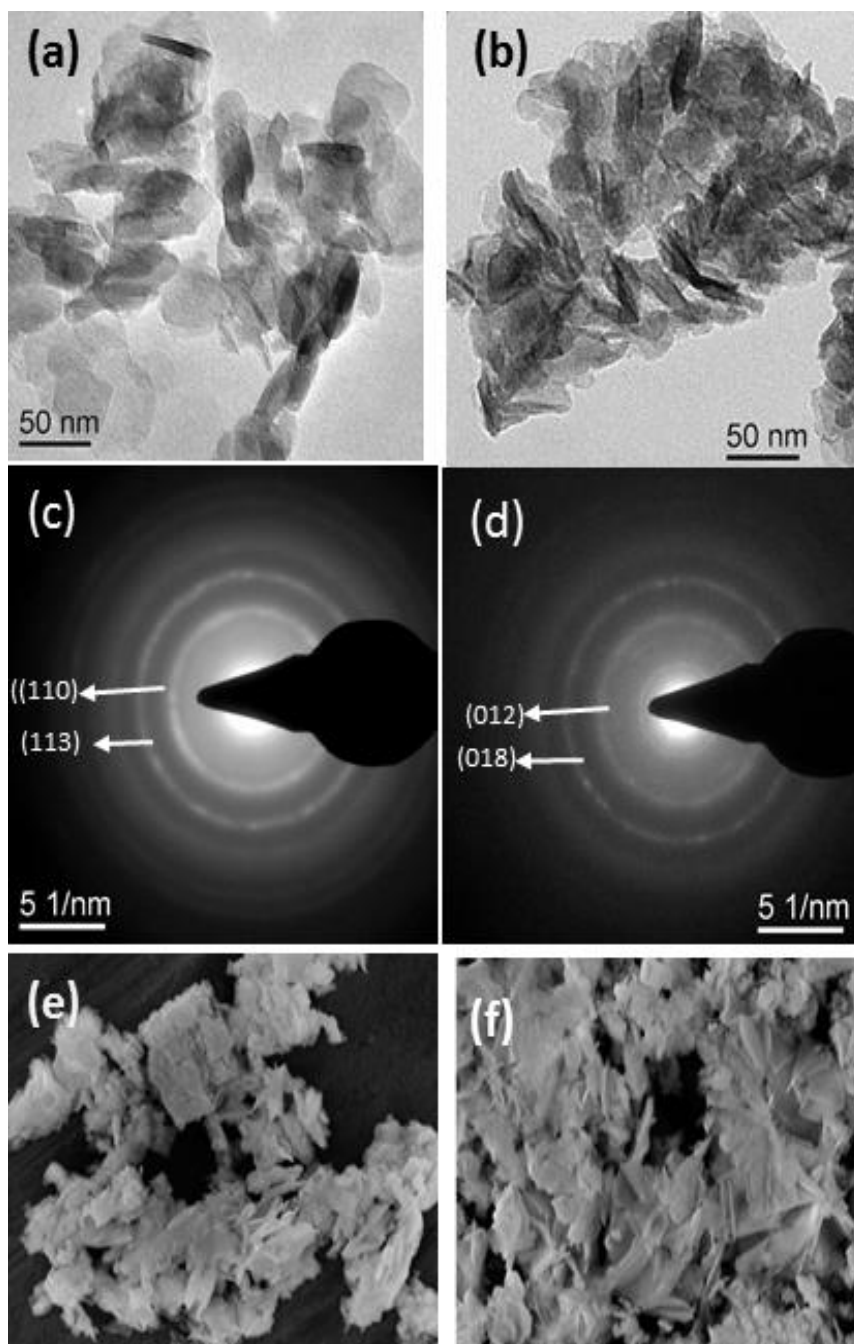


Figure 2. TEM images of (a) Mg/Fe-4 LDH (b) Mg/Fe-4/Mo LDH , SAED patterns of (c) Mg/Fe-4 LDH (d) Mg/Fe-4/Mo LDH, FESEM image of (e) Mg/Fe-4 LDH (f) Mg/Fe-4/Mo LDH.

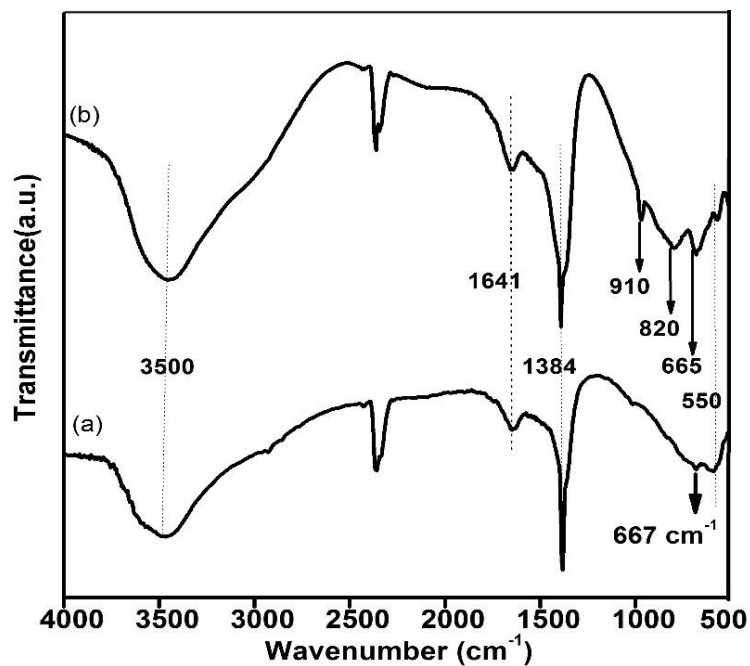


Figure 3. FTIR spectra of (a) Mg/Fe-4 LDH (b) Mg/Fe-4/Mo LDH.

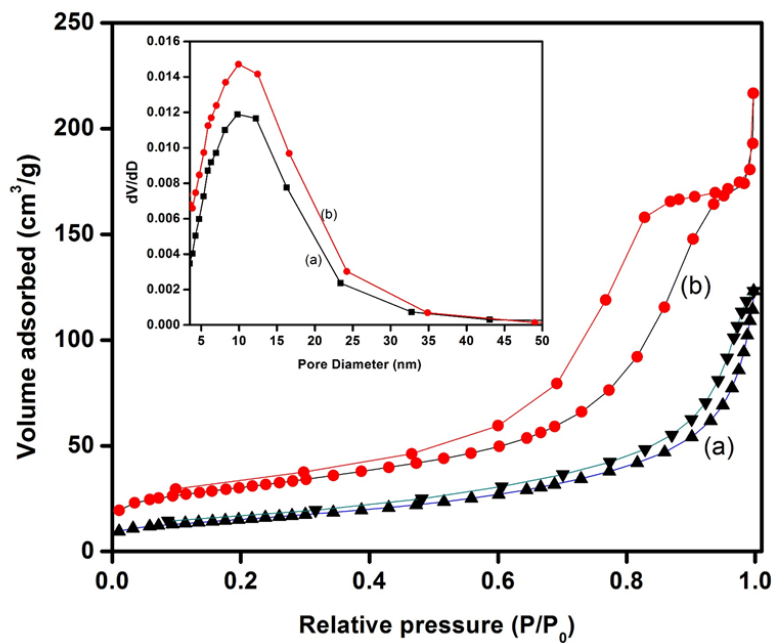


Figure 4. Nitrogen sorption isotherm of (a) Mg/Fe-4 LDH (b) Mg/Fe-4/Mo LDH.

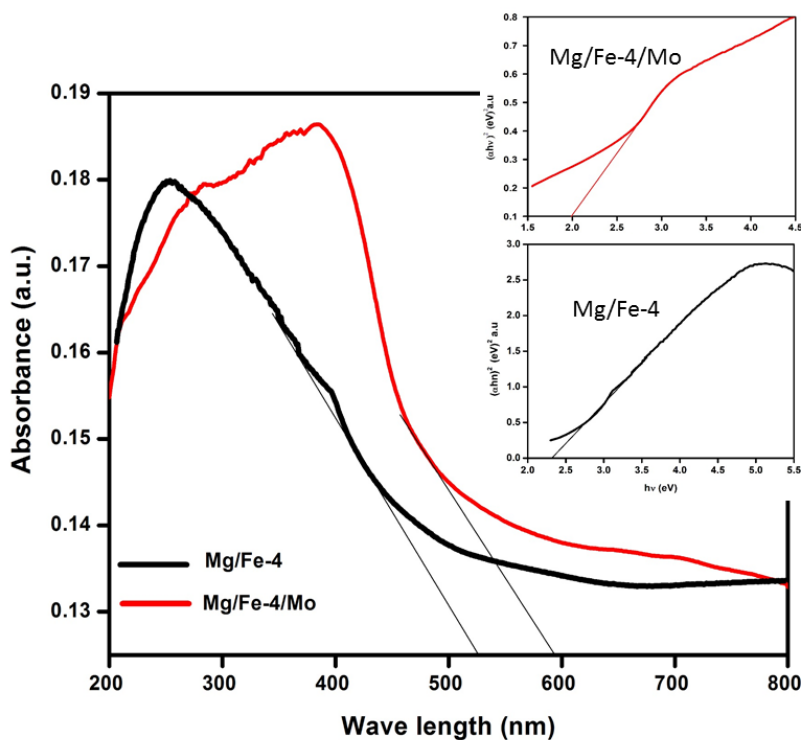


Figure 5. The UV-vis DRS spectra of LDHs (Inset: The specific absorption band edges calculated from DRS).

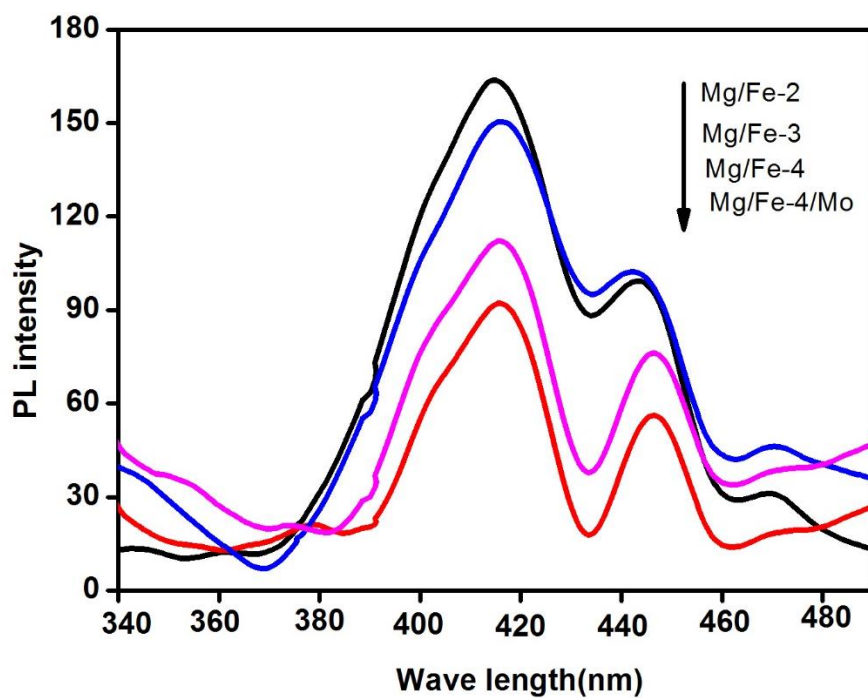


Figure 6. Fluorescence spectra of all the as prepared LDHs.

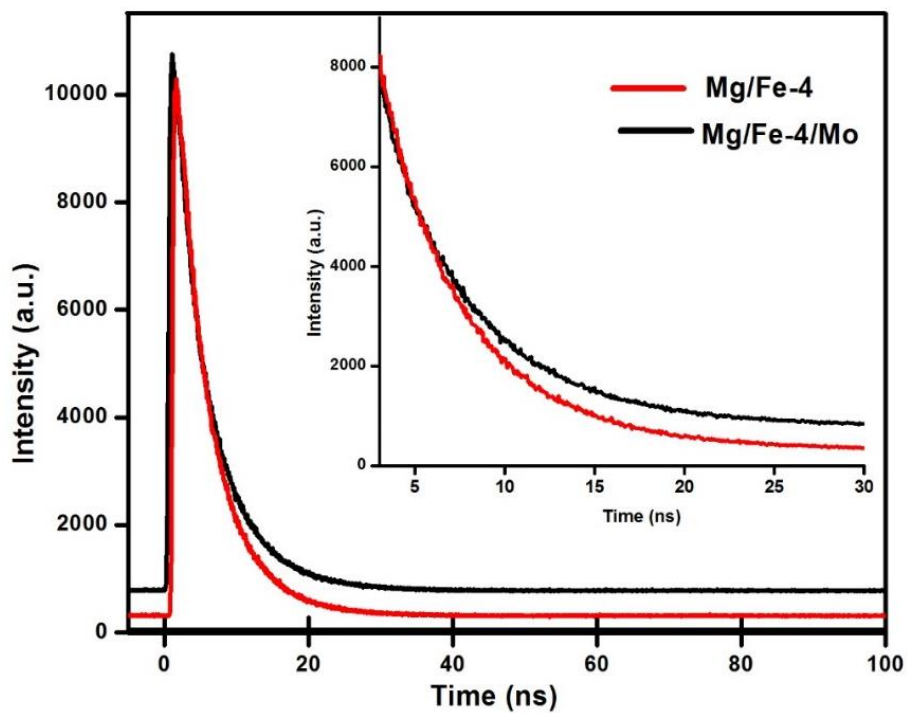


Figure 7. Time-resolved photoluminescence spectra for (a) Mg/Fe-4 LDH (b) Mg/Fe-4/Mo LDH

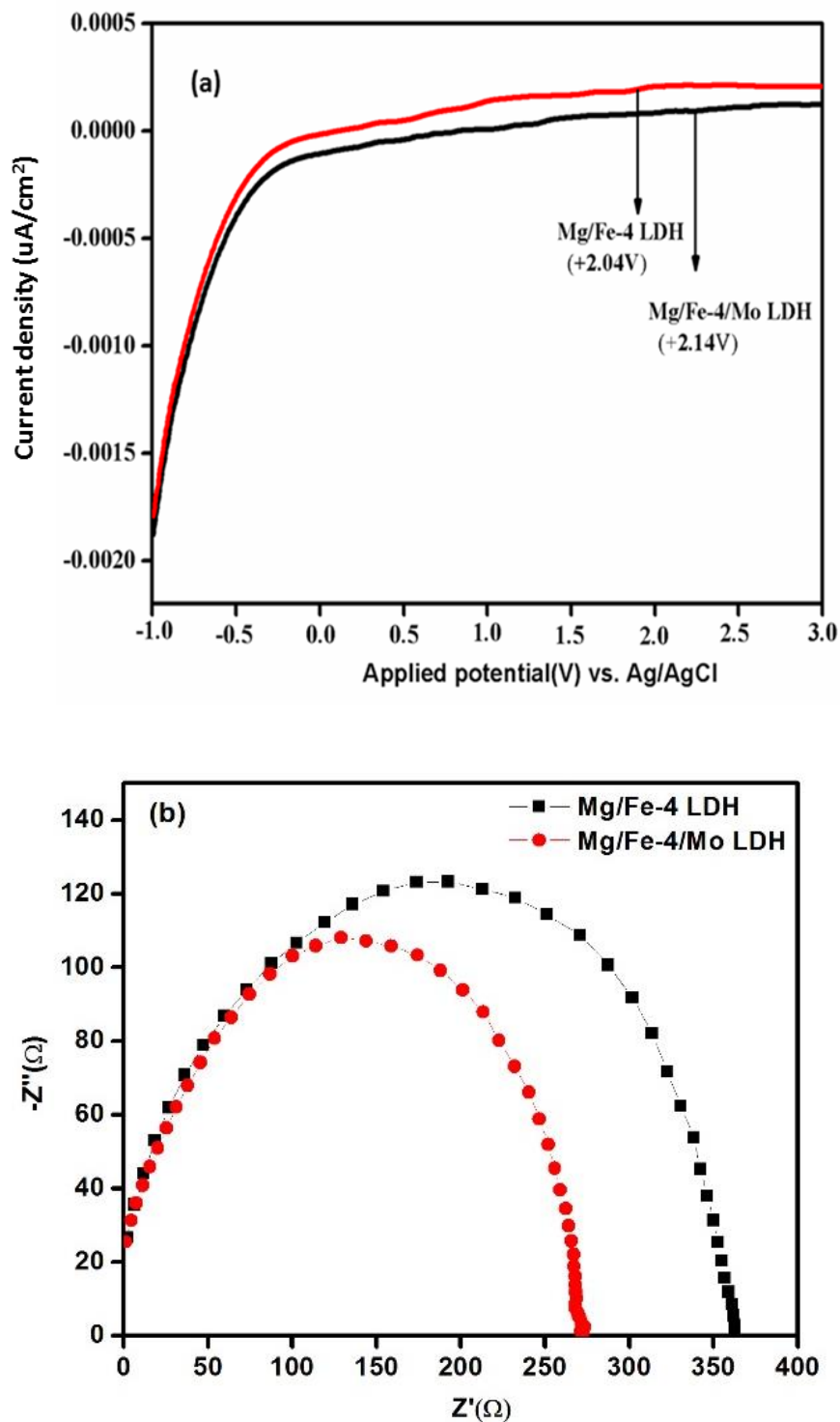
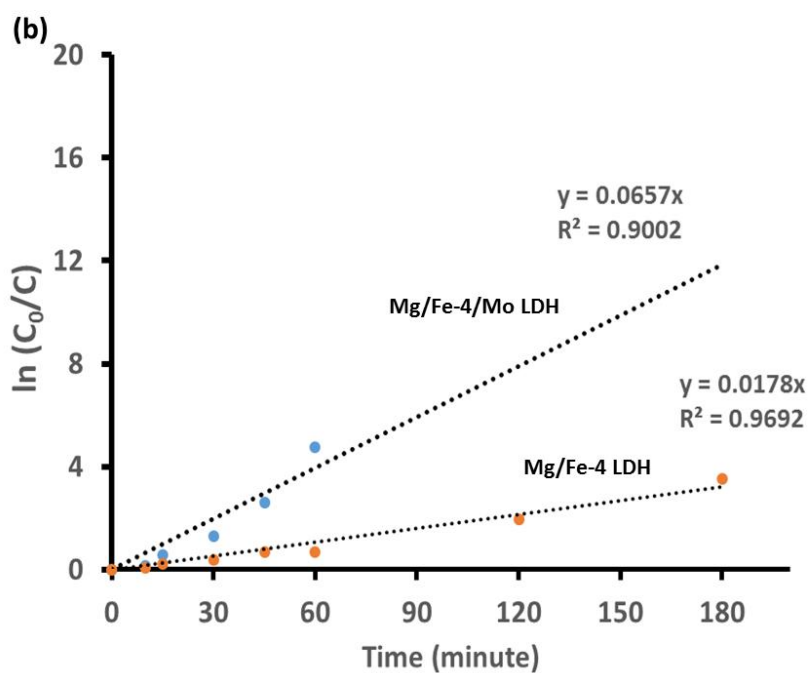
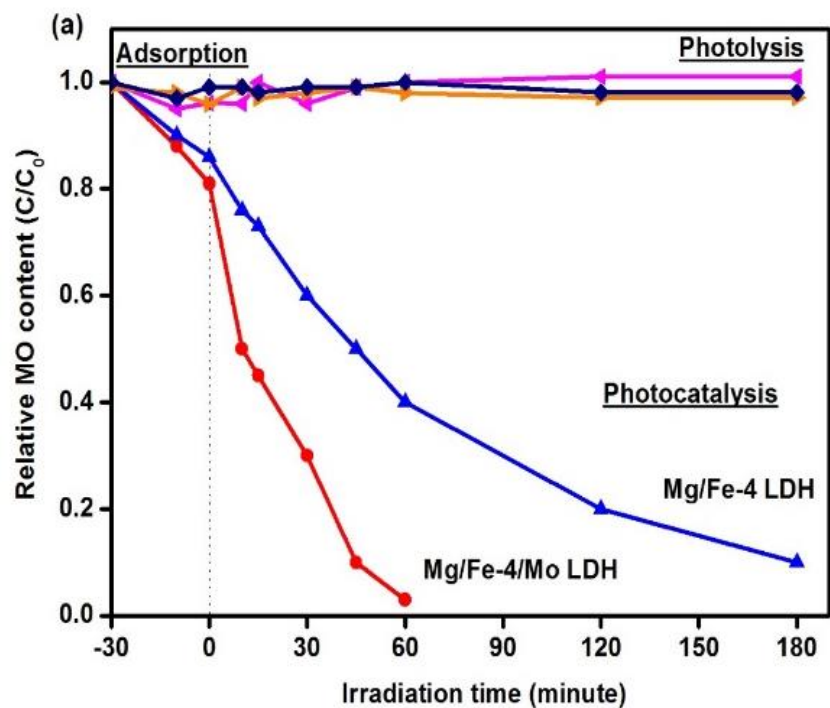


Figure 8. The photocurrent density (I-V) curves and The EIS Nyquist plots of (a) Mg/Fe-4 LDH (b) Mg/Fe-4/Mo LDH.



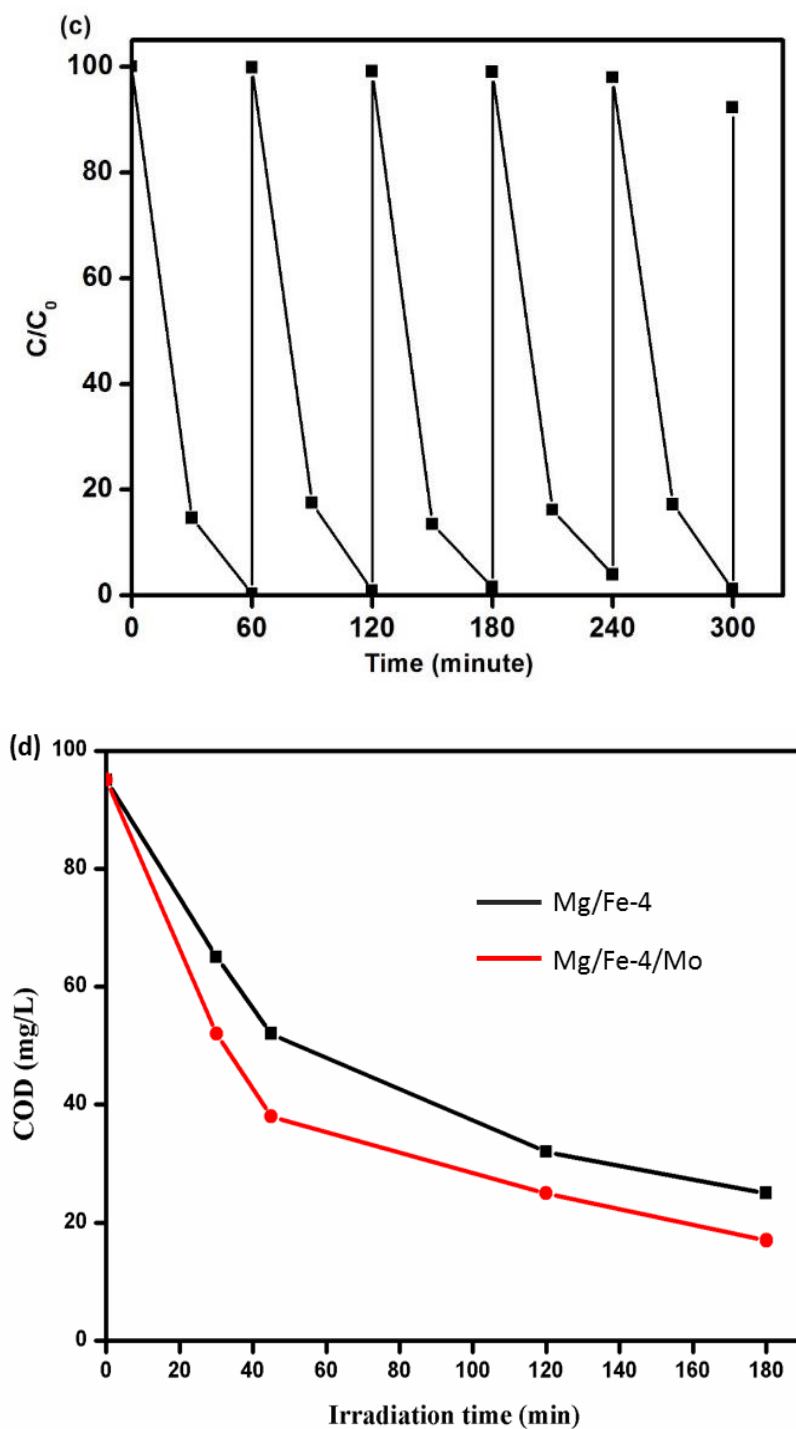


Figure 9. (a) Photocatalytic degradation of MO in aqueous solution over LDHs. (b) Pseudo-first-order kinetics of MO for LDHs. (c) Regeneration study of MO in recycle run over Mg/Fe-4/Mo LDH. (d) Photocatalytic degradation of MO by COD Mg/L.

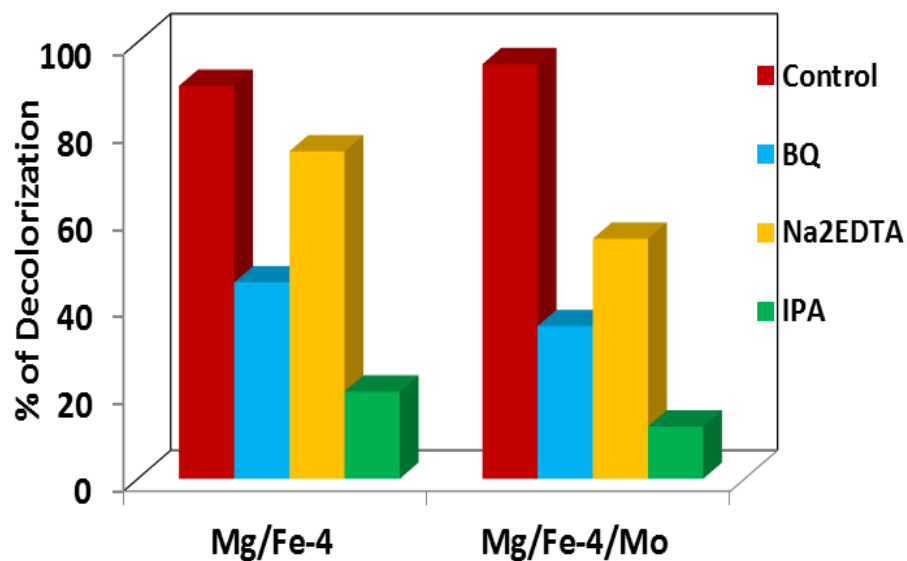


Figure 10. Photocatalysis test by taking different quenchers over Mg/Fe-4 LDH and Mg/Fe-4/Mo LDH.

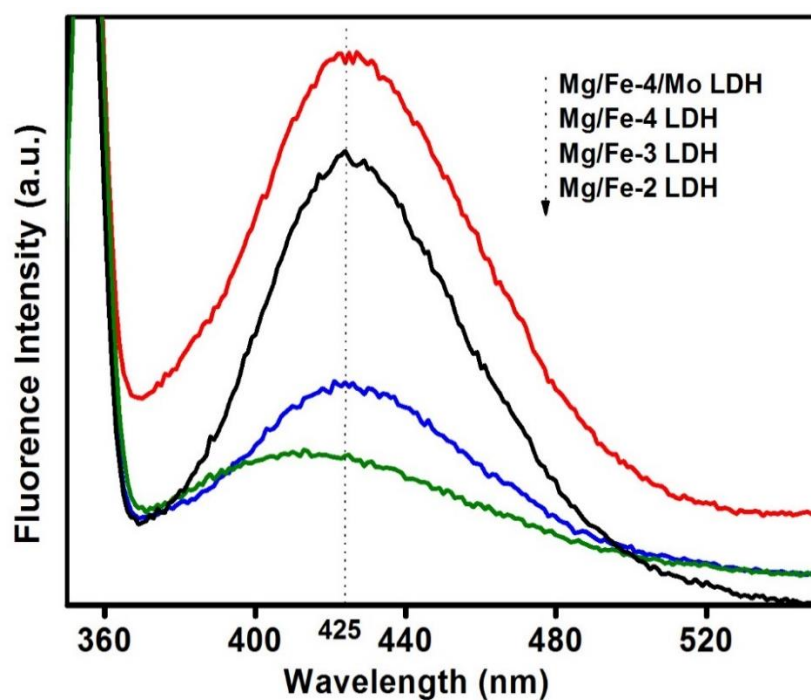
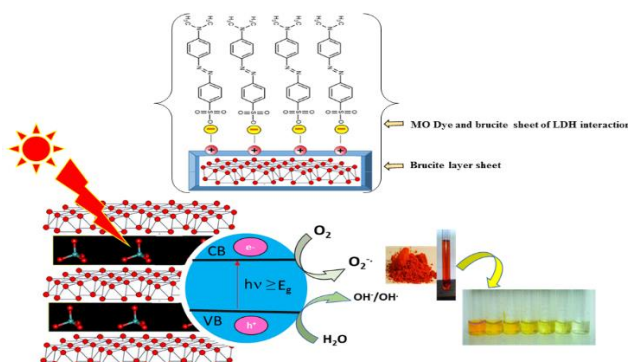


Figure 11. PL spectral changes with visible-light irradiation time over different prepared materials in 5×10^{-5} M basic solution of Terphthalic acid.

Table 1. Photogenerated charge lifetimes of Mg/Fe-4 LDH and Mg/Fe-4/Mo LDH materials.

Samples	A_1	τ_1	A_2	τ_2	τ
Mg/Fe-4 LDH	3496	3.0080	6377.5	6.1634	310
Mg/Fe-4/Mo LDH	3714	3.1951	6497.9	6.2445	980

Table of Contents graphics



Development of a low cost and highly efficient photocatalyst is of great significance in favor of high performance towards photocatalytic organic dye degradation. This work presents the synthesis of Mg/Fe(2:1,3:1,4:1) Layer double hydroxides and modified the more crystalline Mg/Fe (4:1) by intercalating molybdate. The efficient Molybdate intercalated Mg/Fe (4:1) Layered double hydroxide photocatalyst showed excellent activity in a shorter time for degradation of Methyl orange dye. The photocatalytic mechanism was explained on the basis of electrochemical impedance spectroscopy (EIS), photoluminescence (PL) spectra, active trapping measurements and optoelectronic properties. The observed superiority of photocatalyst was mainly attributed to the high band gap energy, prolonged lifetime and faster interfacial charge-transfer rate.